Res. Rep. Fac. Eng. Mie Univ., Vol. 23, pp. 39−50 (1998)

Original Paper

Analysis of Elasto-Plastic Behavior of Concrete-Filled Steel Tubular Beam-Columns Failing in Local Buckling

Akira TSUIKI, Jun KAWAGUCHI, and Shosuke MORINO
(Department of Architecture)

(Received September 14, 1998)

Abstract

Elasto-plastic and post-buckling analysis was performed to trace the cyclic behavior of concrete-filled steel tubular(CFT) beam-columns, which had been tested previously. Analytical model to solve the deflections of the beam-column was divided into a number of elements, and the solution satisfying the equilibrium at each subdivision point was searched by the proposed way of combining the degrading type moment-curvature relation with the numerical integration scheme. The effect of local buckling of steel tube was taken into account by employing the degrading type of stress-stain relation. The paper first presents how to handle the deflection analysis of a member whose moment-curvature relation possesses the descending part, which is not possible by the conventional numerical integration, and discusses the accuracy of the solution compared with the test results.

Key words

Stress degradation, Stress-strain relation, Moment-curvature paths, Beam-column, Elasto-plastic analysis, Hysteresis loop

1. Introduction

The building frame consisting of concrete-filled steel tubular (CFT) columns is one of the hybrid-structures which have been developed recently. The number of construction of CFT system has been increasing because of its earthquake resistance capacity and low cost of construction. The research of CFT system has been covering the behavior of short columns (Fujimoto, et al., 1997 a, b), beam-columns (Inai, et al., 1993, Matsui, et al., 1998, Fujimoto, et al., 1998), connections (Yoshioka, et al., 1998) and frames (Kawaguchi, et al., 1997). The design recommendations for

CFT structures (1997) has been published by Architectural Institute of Japan (AIJ) based on the result of research activity. According to the investigation on the elastic-plastic behavior of CFT beam-columns, the limit of the width-to-thickness ration (D/t) was relaxed to the value equal to 1.5 times that for the bare steel tube, counting the restraining effect of the filled-concrete on the local buckling of the tube in AIJ recommendations (1997). In addition, the filled-concrete can carry the axial load, bending moment and the shear force, and thus the CFT with large D/t may be more effectively used in the real practice. In such a case, the local buckling cannot be avoided under the severe earthquake. The authors (Kawaguchi, et al., 1991, 1992) have been carried out the experimental investigation on the post-local buckling behavior of CFT beam-columns with the experiment parameters of D/t, axial load and displacement amplitude, and estimated the strength deterioration and the energy dissipation capacity. The limits of D/t, axial load and displacement amplitude were proposed based on the strength deterioration after the local buckling, but however, it has been impossible to cover the wide range of the experimental parameters, and thus the simulation by the numerical analysis has been done (Kawaguchi, et al., 1995).

The analysis of the load-displacement behavior of a structural member is usually performed by the numerical integration scheme by dividing the member into a number of elements. The beam-column is divided into small elements along the longitudinal axis, and the horizontal deflection at the top of the column is computed by numerical integration of the curvature which is uniformly distributed in each element. In this method, a certain moment-curvature relation of the cross section is used, which is calculated from the stress-strain relation of material. However, this method of analysis is not applicable to a certain member consisting of a material with unstable stress-strain relation which causes degrading type of moment-curvature relation. When the numerical integration scheme explained above is used for the analysis of the load-displacement relation of a cantilever having a degrading type of moment-curvature relation, the solution depends on the number of subdivide elements. **Figure 1**(a) shows sample results for CFT beam-columns of □-100x100x4.5 with the length 1000mm and

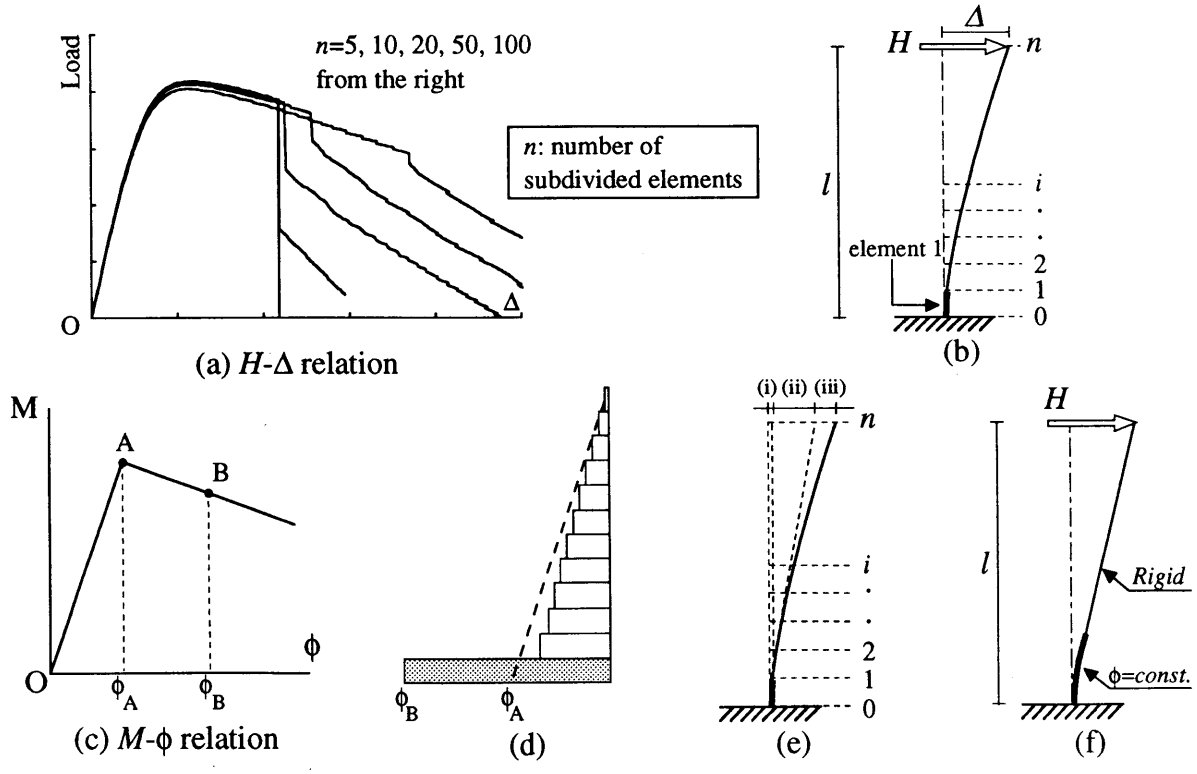

Fig. 1 Problem of the conventional numerical integration scheme

the ratio of axial load to the squash load was 15%. Consider a cantilever subjected to a lateral load H at the tip as shown in **Fig. 1**(b), which has the moment-curvature relation consisting of a linear elastic part and a linear degrading part for simplicity as shown in **Fig. 1**(c). In the course of the numerical integration, it is assumed that the curvature uniformly distributes in each of subdivided elements. When the bending moment at the critical element adjacent to the fixed end, i.e., the element 1 in **Fig. 1**(b), reaches the maximum value indicated by the point A on the moment-curvature relation in **Fig. 1** (c), the load H becomes the maximum, and then the unloading starts. Suppose that the curvature in the element 1 increases to the point B in the subsequent loading process. Since the bending moment along the entire length of the cantilever is reduced, the elastic curvature reversal must occur in all the elements except the element 1, and the curvature distribution becomes as shown in **Fig. 1**(d). The tip deflection Δ at this stage is composed of three components; (i) the deflection of the element 1, (ii) the tip deflection caused by the slope of the element 1, and (iii) the tip deflection caused by the elastic deformation of all the elements except the element 1, as shown in **Fig. 1**(e). Numerically-calculated values of these three components change, depending on the number of the subdivided elements n. As far as n is sufficiently large, the value of the component (i) is negligible, and the component (iii) is nearly equal to the exact solution. However, the value of the component (ii), which is approximately given by $\phi l^2/n$, sensitively depends on n, and it becomes smaller as n increases. These are the explanations to the contradiction observed in **Fig. 1**(a): the solution depends on the value of n, and the slope of the unloading curve becomes steeper as the value of n increases.

This problem has been notified for a long time, but an efficient method of analysis has not yet been found, and a simple method was often taken which assumed a uniform distribution of the curvature in a plastic zone with a finite length in the vicinity of the critical element. Kawaguchi, Morino, Atsumi and Yamamoto (1991) assumed that the deformation occurred only at the base portion of a constant length where the curvature corresponding to the bending moment generated at the base distributed uniformly, and the rest portion was rigid, as shown in **Fig. 1**(f). Inai, Iida and Shimazaki (1993) proposed the model with the plastic zone which took into account of the elaste curvature distribution along the beam-column. However, these curvature distribution along the longitudinal axis in the analysis were quite different from the real one, and the results of analysis were changed according to the length of the plastic zone. Morino, Kawaguchi and Fukao (1995) proposed a method of combining the degrading type of moment-curvature relation with the conventional numerical integration scheme. However, the proposed method was only applicable to the behavior under the monotonic loading, and there was a contradiction that even an elastic portion of the beam-column behaved as if it was in the inelastic range, since it was assumed that the increase in the curvature occurred in every portion after the deterioration started at the critical element. This paper proposes an improved the method of combining the degrading type of moment-curvature relation with the conventional numerical integration scheme, modifies it for the cyclic analysis, and compares the result of analysis with the test result of CFT beam-columns under the cyclic loading.

2. Analysis of CFT beam-columns

2.1 Stress-strain relations

Figure 2(a) shows a degrading type of stress-strain relation which deals with the strength deterioration due to the effect local buckling. The points P, Y, and U indicate proportional limit,

start of strain-hardening in tension and occurrence of local buckling in compression, respectively. The curve consists of linear elastic (point P_t to P_c), curvilinear elasto-plastic transition (P_t to Y and P_c to U), strain-hardening (Y to T) and strength deterioration (U to C) paths. They are given by the following mathematical expressions:

Elastic part

$$\sigma(\varepsilon) = E \times \varepsilon \tag{1}$$

Transition part

$$\sigma(\varepsilon) = \sigma_1(\varepsilon) + \sigma_2(\varepsilon) \tag{2}$$

where

$$\sigma_1(\varepsilon) = \frac{(\varepsilon - \varepsilon_{pc}) \times (\sigma_u - \sigma_{pc}) / (\varepsilon_u - \varepsilon_{pc})}{[1+\{(\varepsilon - \varepsilon_{pc}) / (\varepsilon_u - \varepsilon_{pc})\}^k]^{1/k}} + \sigma_{pc}$$

$$\sigma_2(\varepsilon) = \frac{\sigma_u - \sigma_1(\varepsilon_{cr})}{(\varepsilon_{cr} - \varepsilon_{pc})} \times (\varepsilon - \varepsilon_{pc}) \tag{3}$$

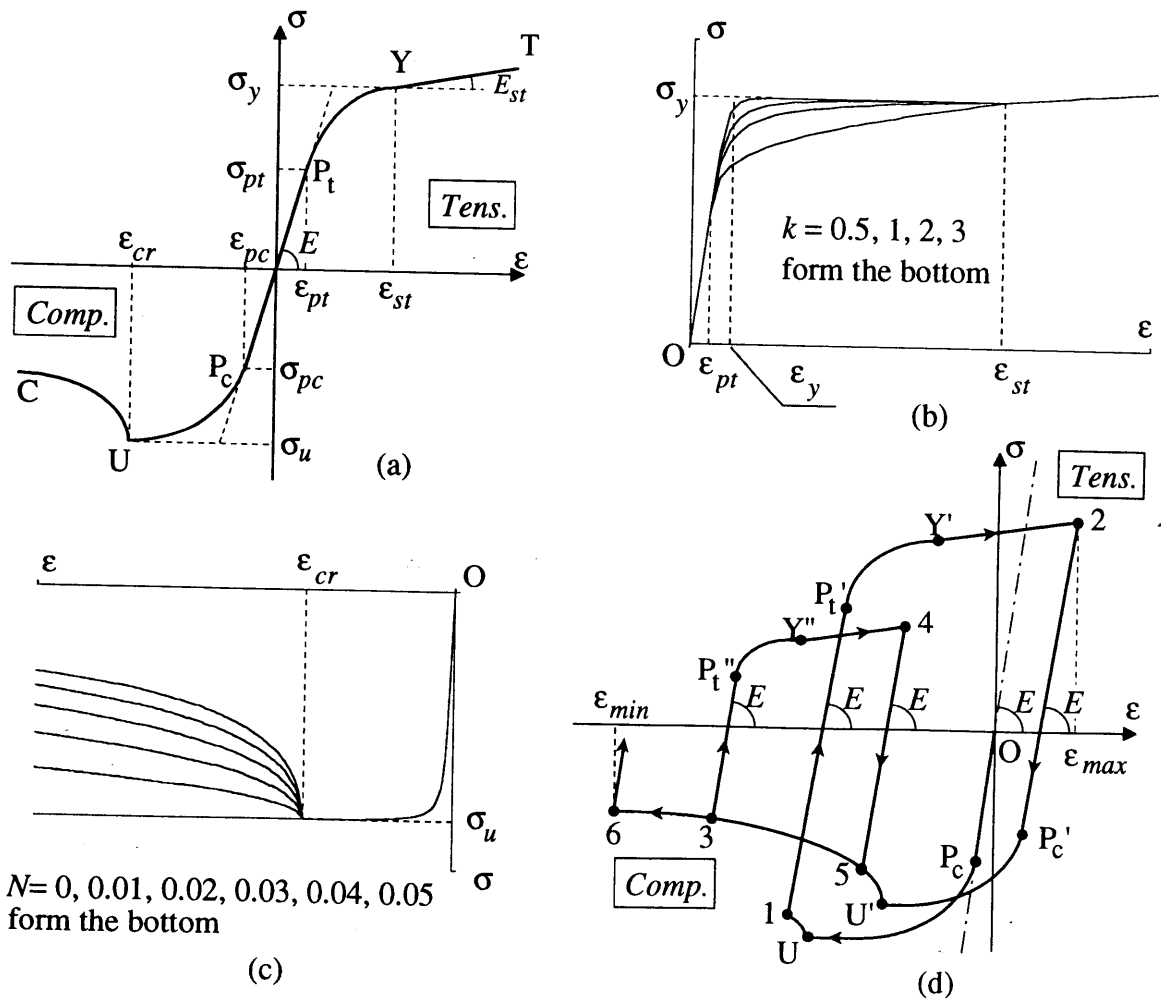

Fig. 2 Stress-strain relations (Steel)

Hardening part

$$\sigma(\varepsilon) = E_{st} \times (\varepsilon - \varepsilon_{st}) + \sigma_y \tag{4}$$

Deterioration part

$$\sigma(\varepsilon) = \{\sqrt{(4\lambda^2 \cdot F^2(\varepsilon) + 1)} - 2\lambda \cdot F(\varepsilon)\} \times \sigma_u \tag{5}$$

where

$$F(\varepsilon) = \sqrt{2 \times (\varepsilon - \varepsilon_{cr}) + (\varepsilon - \varepsilon_{cr})^2} \tag{6}$$

$\lambda = N(D/t)$ D / t : width-thickness ratio

Equation (3) is written for the curve in compression, and subscript *pe* should read *pt*, *u* should read *y*, and *cr* should read *st*, for the curve in tension. The values of *k* should be different for compression and tension. Equations (2) and (3) are derived by modifying an equation proposed by Richard according to Smith (1972), in which the parameter *k* determines the shape of the curve : the curve approaches the ideal elasto-plastic type with the increase of *k* , and the curvature of the curve becomes larger as *k* becomes smaller , as shown in **Fig. 2**(b). On the other hand , the parameter *N* determines the shape of the deterioration curve shown in **Fig. 2**(c) for compression. Equation (5) is derived in view of a technique to replace a locally-buckled plate by a number of buckled bars shown by Morino et al.(1986). Note that the stress-strain relation shown above includes the effect of local buckling in a macroscopic way. It is not for an infinitesimal element, but it should be defined as the force-deformation relation of a bar element with unit area and unit length. The cyclic path of the stress point in a steel segment is shown in **Fig. 2**(d), starting from compression. It turns at point 1 after the local buckling occurs at U, and the stress point follows the linear unloading path and reaches the turning point 2 passing P_t' and Y'. The stress levels at P_t' and Y' are defined, based on the compressive strain ε_{min} at point 1, which is the minimum strain experienced so far , as given by equation (7).

$$\begin{aligned}
&\text{when} \quad \varepsilon_{min} < \varepsilon_{cr} \quad \text{and} \quad |\sigma(\varepsilon_{min})| < \sigma(Y) : \\
&\qquad \sigma(Y') = -\sigma(\varepsilon_{min}) \quad \text{and} \quad \sigma(P_t') = \{\sigma(Y')/\sigma(Y)\} \times \sigma(P_t) \\
&\text{when} \quad \varepsilon_{min} \geqq \varepsilon_{cr} \quad \text{or} \quad |\sigma(\varepsilon_{min})| \geqq \sigma(Y) : \\
&\qquad \sigma(Y') = \sigma(Y) \quad \text{and} \quad \sigma(P_t') = \sigma(P_t)
\end{aligned} \tag{7}$$

The tensile stress-strain relation between P_t' and Y' is generated from equations (2) , (3) and (7) by replacing σ_{pt} and σ_y by $\sigma(P_t')$ and $\sigma(Y')$, respectively, and by shifting the value of the strain by the amount of $\sigma(\varepsilon_{min})/E$-$\varepsilon_{min}$. New proportional limit P_c' and local buckling strength U' in the second cycle of the compression side are similarly determined depending on the maximum tensile strain ε_{max} experienced at the turning point 2 as follows:

$$\begin{aligned}
&X = \sigma(\varepsilon_{max})/E - \varepsilon_{max} \\
&\text{when} \quad X < 0 : \quad \sigma(U') = 1.4^{X/\varepsilon_{cr}} \times \sigma(U) \quad \text{and} \quad \sigma(P_c') = \{\sigma(U')/\sigma(U)\} \times \sigma(P_c) \\
&\text{when} \quad X \geqq 0 : \quad \sigma(U') = \sigma(U) \quad \text{and} \quad \sigma(P_c') = \sigma(P_c)
\end{aligned} \tag{8}$$

The stress-strain relation proposed by Popovics (1971) was employed for the skeleton curve of

the filled-concrete up to the maximum strength, and it was assumed that the maximum strength was sustained by the confining effect of the steel tube , as given by equation (9).

$$\begin{aligned} &\text{when } 0 \leqq \varepsilon \leqq \varepsilon_m : \quad \sigma(\varepsilon) = \frac{F_c \cdot Na}{Na - 1 + (\varepsilon / \varepsilon_m)^{Na}} \times \frac{\varepsilon}{\varepsilon_m} \\ &\text{when } \varepsilon_m < \varepsilon : \quad \sigma(\varepsilon) = \sigma(\varepsilon_m) = F_c \\ &\text{where} \quad Na = 0.00571 \cdot F_c + 1 \qquad F_c : \text{cylinder strength} \end{aligned} \tag{9}$$

The tensile stress was neglected in the skeleton curve. The cyclic rules for the concrete has been constructed based on the model proposed by Fujii, et al. (1973) as shown in **Fig. 3**, in which three types of the stress-strain paths are shown: path I (A → B → C → D → C → A), path II (A' → B' → C' → D' → E), and path III (A" → B" → C" → A"). General rules are as follows: i) If the strain at the first turning point is larger than ε_E, the path comes back to the first turning point, as in the case of the paths I and III. The value of ε_E is given by F_c/E_c, where F_c and E_c denote the cylinder strength and the elastic modulus of concrete; ii) If the strain at the first turning point is smaller than ε_E, the path comes back to the point E at which the value of strain is equal to ε_E, as in the case of the path II; iii) In the process of strain reversal, the stress decreases linearly with the modulus E_c until the stress level becomes equal to 1/4 of the stress at the respective turning point, and then the slope changes to $E_c/4$, as in the path A → B → C; and iv) The concrete does not carry the tensile stress, as in the path C → D.

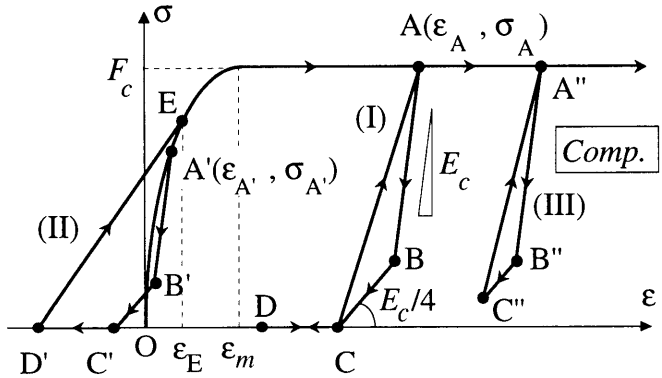

$$E_c = 2.1 \times 10^5 \times \sqrt{\frac{F_c}{200}}$$

$$\varepsilon_E = F_c / E_c$$

Fig. 3 Stress-strain relations (Concrete)

2.2 Analysis of load-displacement relations

The load-displacement relation of a cantilever was analyzed by the numerical integration scheme. The model cantilever of length l is shown in **Fig. 4** (a), which is subjected to the constant vertical load P and the horizontal load H at the top. It was divided into n elements of equal length a. As discussed in detail below, a conventional numerical integration scheme cannot be directly applied to analyze the load-displacement relation of a cantilever having a degrading type of moment-curvature relation. Therefore, in the present analysis, the cantilever was divided into a number of elements and modified moment-curvature relation was assigned to each element, of which details are discussed in the next section. The solution satisfying the equilibrium at each subdivision point was searched numerically, based on the assumption that the curvature was uniformly distributed in each of subdivided elements. In the process of

determining the deflected shape of the cantilever, a trial-and-error procedure was required, since the equilibrium of the bending moment involved $P\Delta$ moment. In order to avoid this tediousness, the $P\Delta$ moment was assumed to distribute linearly along the member axis as shown in **Fig. 4** (b)

2.3 Monotonic moment-curvature path

Main feature of the present analysis method is based on the assumption that each subdivided element of the cantilever follows its own moment-curvature path which is different from others. Consider the moment(M)-curvature(ϕ) relation consisting of a linear elastic part (OP), curvilinear inelastic(PB) and degrading(BC) parts as shown in **Fig. 5** (a). When the bending moment at the critical element adjacent to the fixed end, i.e., the element 1 in **Fig. 4** (a), reaches the maximum value indicated by the point B on the moment-curvature relation in **Fig. 5** (b), the load H becomes the maximum, and then the unloading starts. When the M-ϕ point of the critical element moves from the point B to C in **Fig. 5** (b), the M-ϕ points in other elements are assumed to move from the point B' to C', B" to C", and so forth, on the lines connecting the points A and B' or B", respectively. The point A is the intersection of the lines BC and OP (P: elastic limit). Since the bending moment diagram should be linear as shown in **Fig. 4** (b), the values of the bending moment at the points C' and C" are uniquely determined from that at the point C. The M-ϕ point of the element at the point P also moves to the point P'. Note that the elastic strain reversal occurs in the element which remained elastic when the strength deterioration occurred in the critical element, and all other inelastic elements follow different M-ϕ paths.

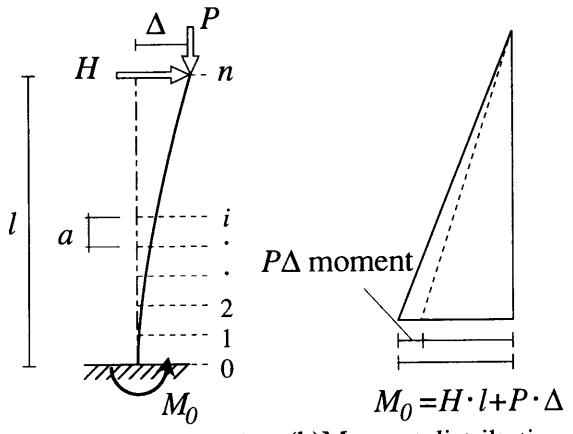

Fig. 4 Analytical model

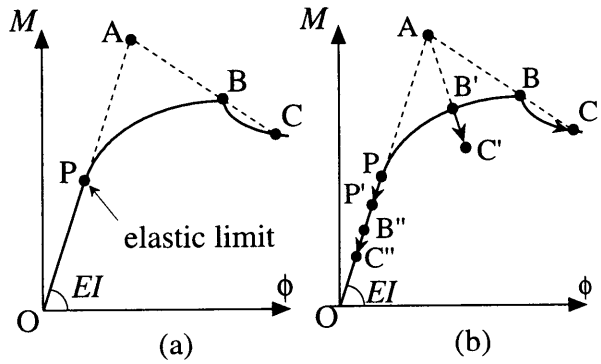

Fig. 5 Monotonic moment-curvature path

2.4 Cyclic moment-curvature path

The moment -curvature relation of the critical element under the cyclic loading can be calculated from the stress-strain relations of materials shown in **Fig. 2** and **Fig. 3** by a conventional procedure, and let us call this relation as the "original M-ϕ" relation. The cyclic moment-curvature paths of other elements are shown in Fig. 4. When the M-ϕ point of the critical element reaches the point C, the M-ϕ points of other two elements are at the points C' and C", in general, and they move to the points D' and D", respectively, as the M-ϕ point of the critical element moves from the point C to D according to the original M-ϕ relation. The movement of the M-ϕ point of a

general element was defined as follows:

1) If the element is in the elastic range (point C" in **Fig. 6** (a)) when the M-ϕ point of the critical element reaches the turning point C, the M-ϕ point of this element moves on the elastic line (C" → D"), where the value of the bending moment is determined by the linear bending moment diagram based on the value at the point D. The mathematical expressions of the M-ϕ point of this case are given as follows:

$$\phi_{D"} = \frac{1}{EI}\left(M_{C"} \times \frac{M_D}{M_C}\right) \quad , \quad M_{D"} = M_{C"} \times \frac{M_D}{M_C} \tag{10}$$

which means that the elastic element remains elastic from beginning to end of the cyclic loading.

2) If the element is in the inelastic range (point C' in **Fig. 6** (b)) when the M-ϕ point of the critical element reaches the turning point C, the movement of the M-ϕ point of this element is assumed to be controlled by the positions of fictitious points X and X', both of which are on the elastic line OP, and determined in the following manner. First, the point X is defined as the intersection of the elastic line OP and the line CC'. The position of the point X' is determined so that the following proportionality is satisfied:

$$M_1 : M_2 = M_1' : M_2' \tag{11}$$

where M_1, M_2, M_1' and M_2' are the difference between the moment values at the point C and X, at the point X and P', at the point D and X', and at the point X' and P", respectively. The point P' is in the elastic range, and thus the position of P" is already determined in the step 1) above, depending on the movement of the point C to D. The expressions for the bending moment and the curvature at the point X' are given as follows:

$$\phi_{X'} = \frac{\alpha \cdot \phi_C - M_C}{\alpha - EI} \times \frac{M_D}{M_C} \quad , \quad M_{X'} = EI \cdot \frac{\alpha \cdot \phi_C - M_C}{\alpha - EI} \times \frac{M_D}{M_C} \tag{12}$$

$$\text{where} \quad \alpha = \frac{M_C - M_{C'}}{\phi_C - \phi_{C'}}$$

The point D' is assumed to be on the line DX', and the value of the bending moment at the point D' is also determined by the linear bending moment diagram based on the value at the point D.

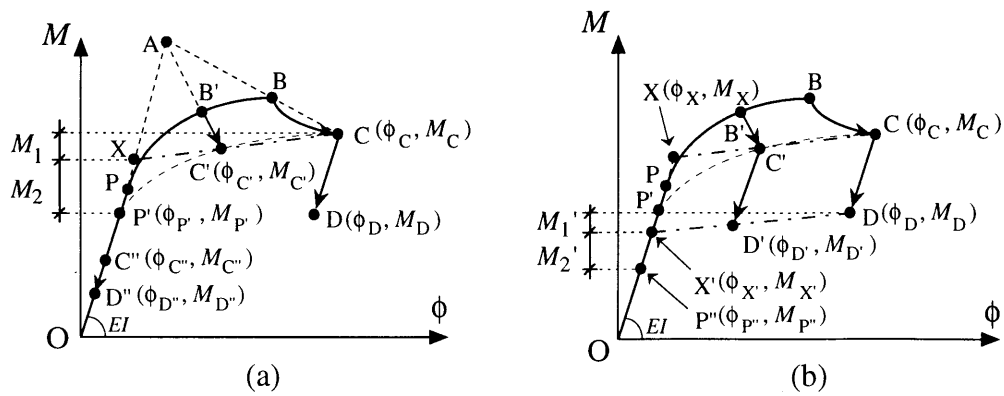

Fig. 6 Cyclic moment-curvature path

The expressions for the bending moment and the curvature at the point D' are given as follows:

$$\phi_{D'} = (M_{C'} - M_C) \cdot \frac{\phi_D - \phi_{X'}}{M_D - M_{X'}} \times \frac{M_D}{M_C} + \phi_D \quad , \quad M_{D'} = M_{C'} \times \frac{M_D}{M_C} \qquad (13)$$

3. Results and discussion

The post local buckling behavior of cantilever beam-columns with CFT or square hollow sections was experimentally investigated by the authors (1992). The cross-section was □-100x100x3 with or without filled-concrete, and the length l was 100 cm. The ratio of axial load to the squash load was 15 %. Ten cycles of loading with the constant displacement amplitude were applied to the specimen. The monotonic and cyclic analyses were performed for the tested specimens, using the material properties shown in **Table 1**, which defined the stress-strain relations of the analytical model.

Figure 7 shows the results of the monotonic analysis to verify the uniqueness of the solution. It is observed in **Fig. 7** (a) that the solutions do not depend on the number of elements n, if the value of n is sufficiently large. The M-ϕ paths of 1st, 3rd and 50th elements from the

Table 1 Material properies

	CFT	Square hollow
E (kN/mm^2)	171	200
E_{st}/E	0.01	0.01
σ_{pt} (N/mm^2)	196	196
σ_{pc} (N/mm^2)	-196	-196
σ_y (N/mm^2)	324.4	398.9
σ_u (N/mm^2)	-413.6	-386.1
ε_{st} (%)	1.6	1.6
ε_{cr} (%)	3.6	2.5
k (tens.)	1.5	1.5
k (comp.)	1.3	1.1
N	0.04	0.06
F_c (N/mm^2)	22.6	
ε_m (%)	0.2	

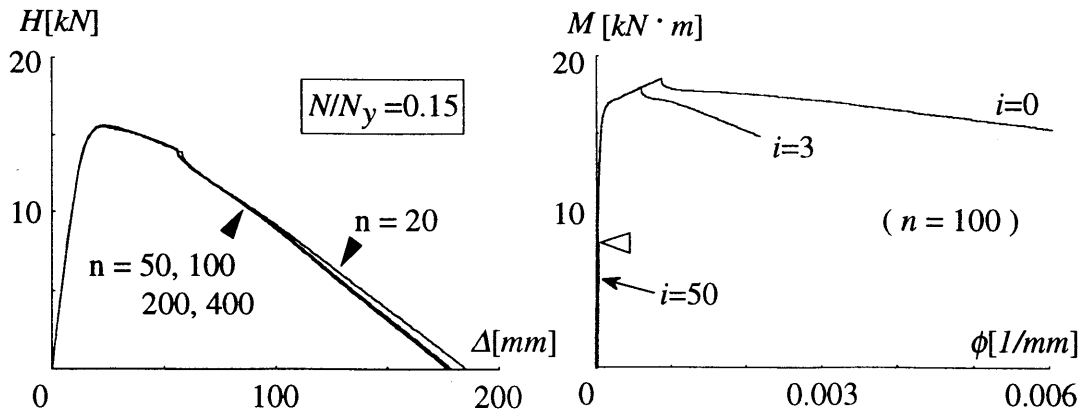

(a) Load-deflection relation (b) Moment-curvature relation

Fig. 7 Results of analysis: Monotonic loading

base in the case of n = 100 are shown in **Fig. 7** (b), which indicates that the M-ϕ path is all different for each of the inelastic elements, and the elastic reversal occurs in the 50th element (midheight element) at the point marked by a triangle.

Figure 8 shows the load-displacement relations in the first loading cycle, and the moment-curvature paths of the 1st, 3rd and 50th elements from the base in the first loading cycle, both of which were obtained from the analysis for the tested CFT specimen. It is observed that the analytical results do not depend on the number of elements n, and the 50th element behaves elastically, as in the case of the monotonic loading shown in **Fig. 7**. **Figure 9** shows the comparison of the load-displacement relations obtained from the test and the analysis. The analytical results show more rectangular shape of the hysteresis loops compared with the test

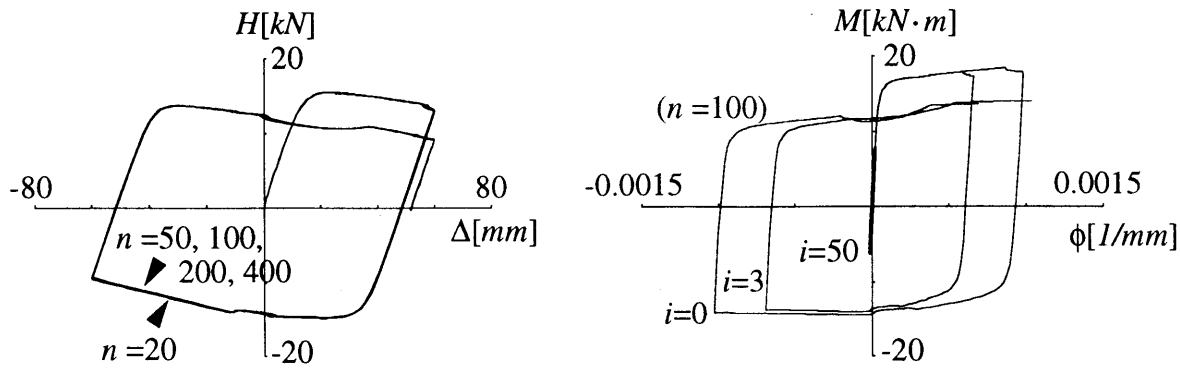

(a) H-Δ relation (b) M-ϕ relation

Fig. 8 Results of analysis: Cyclic loading

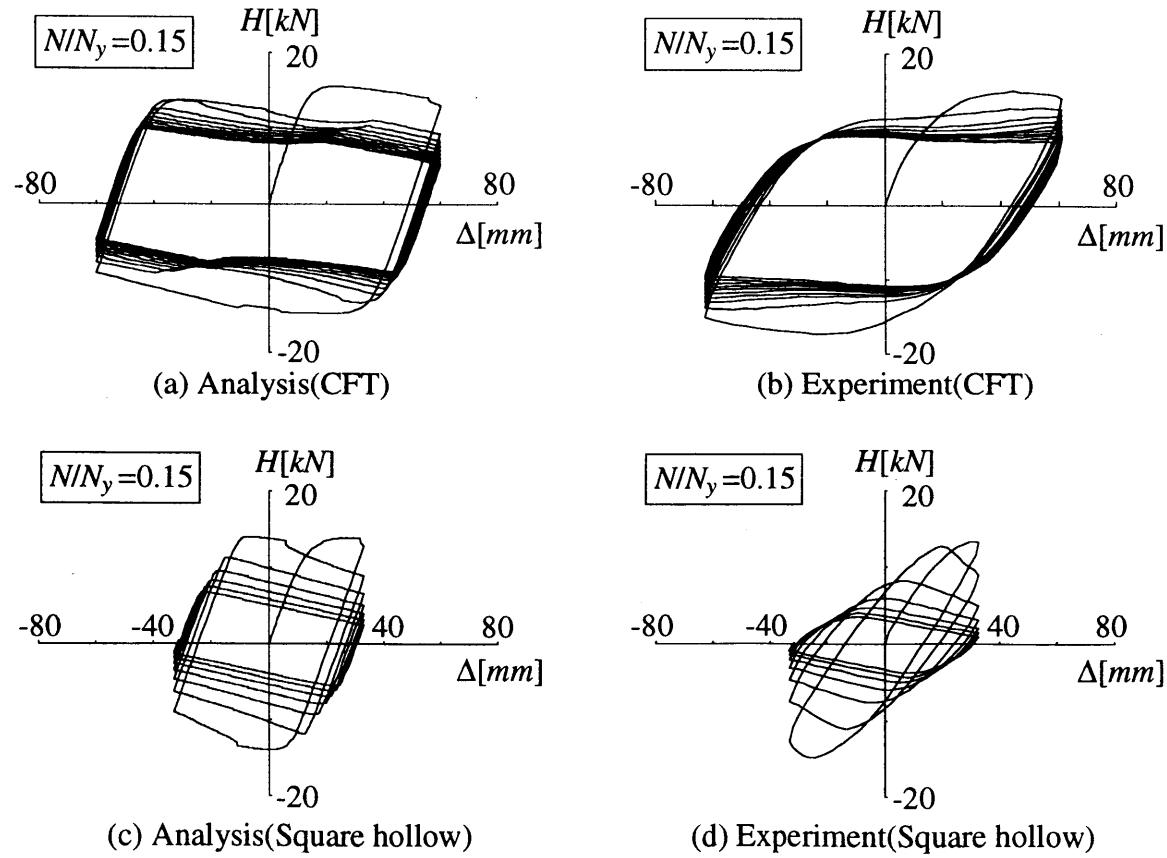

(a) Analysis(CFT) (b) Experiment(CFT)

(c) Analysis(Square hollow) (d) Experiment(Square hollow)

Fig. 9 Comparison of load-displacement relations

results, since the Bauschinger's effect on the stress-strain relation of steel was not properly considered. However, strength deterioration behavior due to the cyclic loading, and the pinching of the hysteresis loops in the case of CFT due to filled concrete were well reproduced by the analysis. The hysteresis loops seem to converge in the case of the CFT specimen, while they shrink continuously in the case of the specimen with a hollow section, and this convergence-divergence phenomena were also captured by the analysis. **Figure 10** shows the change of the curvature distribution along the beam-column in the first loading cycle. The vertical axis and the horizontal axis show the member axis and the curvature, respectively. **Figure 10** (a) shows the curvature distribution at the first turning point of loading, i.e., the point (a) on the moment-curvature curve. **Figure 10** (b) shows the zero moment point at (b), where the residual curvature appears. **Figure 10** (c) shows the state when the curvature at the base element becomes equal to zero at point (c), the curvature of other parts enter into the positive side. These curvature distribution seems very similar to the real one.

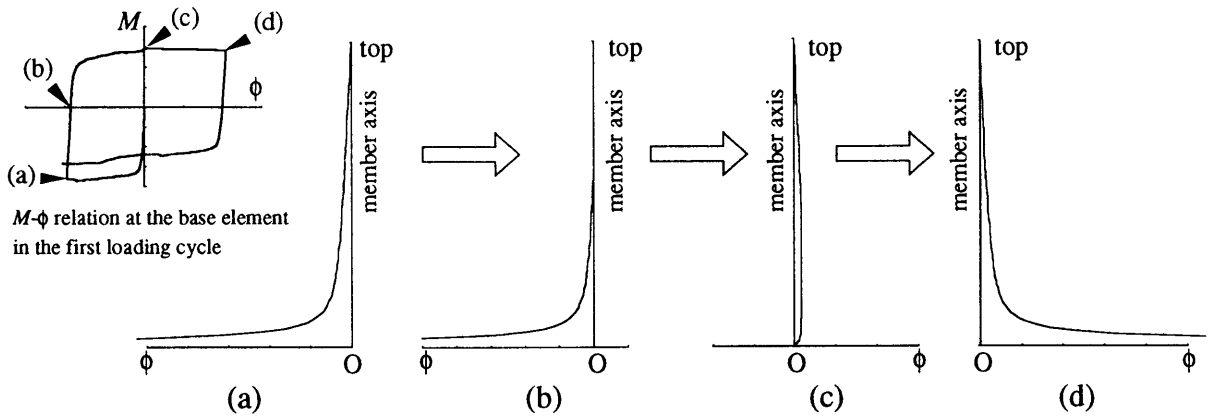

Fig. 10 Change of Curvature Distribution

4. Concluding remarks

Elasto-plastic behavior of CFT beam-columns failing in local buckling under the cyclic loading was analyzed, and the results were compared with test results previously obtained. The method of cyclic analysis, which used the numerical integration scheme together with a proposed way of allowing different cyclic moment-curvature path in each of the subdivided elements, was applicable to a beam-column with a degrading type of moment-curvature relation, and the solution was independent of the number of subdivided elements. The analysis well traced the characteristics of the test results, such as the strength deterioration due to the cyclic loading, the pinching of the hysteresis loops due to filled-concrete, and the convergence-divergence of the hysteresis loops, but the analytical results showed more rectangular shape of the hysteresis loops compared with the test results.

References

[1] S. Popovics, *Factors Affecting the Elastic Deformations of Concrete*, Proc. of the International Conference on Mechanical Behavior of Materials, Kyoto, IV, pp. 172-183, 1971.

[2] J. H. Smith, *Nonlinear Beam and Plate Elements*, Proc. of ASCE, Journal of Structural Division, Vol. 98, No. ST3, pp. 555-571, 1972.

[3] S. Fujii, H. Aoyama and K. Umemura, *Moment-Curvature Relation of Reinforced Concrete*

Cross Section Based on Material Characteristics, Summaries of Technical Papers of Annual Convention, Architectural Institute of Japan, pp. 1261-1262, Oct., 1973.
[4] S. Morino, C. Matsui, and S. Yoshikai, *Local Buckling of Steel Elements in Concrete Encased Columns*, Proc. of Pacific Structural Steel Conference I, Auckland, Vol. 2, pp. 319-335, Aug., 1986.
[5] J. Kawaguchi, S. Morino, H. Atsumi and S. Yamamoto, *Strength Deterioration Behavior of Concrete-Filled Steel Tubular Beam-Columns Under Repeated Horizontal Loading*, Proc. of 3rd International Conference on Steel-Concrete Composite Structures, pp. 119-124, Fukuoka, Japan, Sep., 1991.
[6] J. Kawaguchi, S. Morino, H. Atsumi and S. Yamamoto, *Strength Deterioration Behavior of Concrete-Filled Steel Tubular Beam-Columns*, Proc. of an Engineering Foundation Conference on Composite Construction in Steel and Concrete II, Potosi, ASCE, pp. 825-839, Jun., 1992.
[7] E. Inai, T. Iida and K. Shimazaki, *Analytical Study on the Elasto-Plastic Behavior of Concrete Filled Steel Tubular Columns*, Summaries of Technical Papers of Annual Convention, Architectural Institute of Japan, pp. 1769-1770, Sep., 1993.
[8] S. Morino, J. Kawaguchi and H. Fukao, *Analysis of Elasto-Plastic Behavior of Beam-Columns Failing in Local Buckling*, Proc. of International Conference on Structural Stability and Design, Sydney, pp. 181-186, Oct., 1995.
[9] J. Kawaguchi, S. Morino and T. Machida, *Strength Deterioration Behavior of Locally Buckling CFT Beam-Columns*, Proc. of the 3rd Symposium on Research and Application of Composite Constructions, Nagoya, Japan, pp. 125-130, Nov., 1995.
[10] T. Fujimoto, A. Mukai, I. Nishiyama, E. Inai, M. Kai, Y. Tanaka, H. Tokinoya, T. Noguchi, T. Baba, N. Fukumoto, Y. Murata, K. Sakino and S. Morino, *Axial Compression Behavior of Concrete Filled Steel Tubular Stub Columns Using High Strength Materials*, Journal of Structural and Construction Engineering (Transactions of AIJ), No. 498, pp. 161-168, Aug., 1997 a.
[11] T. Fujimoto, A. Mukai, I. Nishiyama, T. Noguchi, T. Baba, K. Sakino and S. Morino, *Eccentric Compression Test of Concrete Filled Square Steel Tubular Stub Columns Using High Strength Materials*, Journal of Structural and Construction Engineering (Transactions of AIJ), No. 501, pp. 173-180, Nov., 1997 b.
[12] J. Kawaguchi, S. Morino, T. Sugimoto and J. Shirai, *Study on Elasto-Plastic Behavior of Portal Frames Consisting of Square CFT Columns*, Journal of Constructional Steel, Vol. 5, pp. 101-108, Nov., 1997.
[13] Architectural Institute of Japan, *Recommendations for Design and Construction of Concrete Filled Steel Tubular Structures*, 1997.
[14] C. Matsui, K. Tsuda, Y. Yamaji and T. Fujinaga, *Structural Performance and Axial Load Limit of Concrete Filled Steel Square Tubular Columns*, Journal of Structural and Construction Engineering (Transactions of AIJ), No. 504, pp. 103-110, Feb., 1998.
[15] T. Fujimoto, A. Mukai, I. Nishiyama, E. Inai, M. Kai, H. Tokinoya, T. Baba, T. Fukumoto, K. Mori, K. Sakino and S. Morino, *Shear-Flexural Behavior of Concrete Filled Steel Tubular Beam-Columns Using High Strength Materials*, Journal of Structural and Construction Engineering (Transactions of AIJ), No. 509, pp. 167-174, Jul., 1998.
[16] Yoshioka, et al., *U.S.-Japan Cooperative Structural Research Project on Composite and Hybrid Structures -Experiment of CFT Column-Steel Beam Connections-, CFT-25 - CFT-32*, Summaries of Technical Papers of Annual Convention, Architectural Institute of Japan, pp. 1209-1224, Sep., 1998.